Journal of Science and Technology in Civil Engineering, NUCE 2021. 15 (1): 14–29

STRESS-INDEPENDENT PARAMETERS FOR STRESS-STRAIN RELATIONSHIP AND DAMPING IN NONLINEAR ONE-DIMENSIONAL SEISMIC SITE RESPONSE ANALYSIS

Nghiem Manh Hien[a,*]

[a]*College of Information Technology and Engineering, Marshall University, John Marshall Drive, Huntington, WV 25755, USA*

Article history:
Received 24/07/2020, Revised 24/11/2020, Accepted 24/11/2020

Abstract

The modulus reduction and damping curves represent the nonlinear behavior of soil under cyclic load. In the literature, those curves were produced from lab tests of soil at particular confining stresses. This study developed a set of parameters that can be used to normalize the modulus reduction and damping curves to be stress-independent. The proposed formulations for the stress-independent parameters were implemented in the finite element code SRAP and validated through producing shear modulus reduction and damping curves that match the existed ones. Nonlinear 1D seismic site response analyses were conducted for centrifuge experiments to verify the developed computer code. Comparisons of the analysis results between SRAP and another computer code were presented in terms of maximum and minimum displacement, peak ground acceleration, maximum shear strain profiles, and response spectra.

Keywords: backbone curve; hysteretic damping; dynamic soil model; stress-independent parameters; finite element method; nonlinear 1D seismic site response analysis.

https://doi.org/10.31814/stce.nuce2021-15(1)-02

1. Introduction

During the propagation of the seismic wave in soil deposits, the characteristics of strong ground motion, amplitude, frequency content, and duration, are altered because of the influence of local geologic and soil conditions commonly referred to as local site effects [1]. The local site effects were mainly dependent on the geometry and material properties of the subsurface, site topography, and characteristics of the input motion. They can be illustrated by theoretical site response analysis and field measurements. In the theoretical analysis methods, one-dimensional site response analysis methods were widely used and suitable to solve the problem of vertical propagation of a horizontal shear wave through a horizontally layered soil deposit in both frequency and time domains. However, when the bedrock of subsurface deposits forms a basin, two-dimensional (2D) or three-dimensional (3D) analysis is preferred.

Nonlinear site response is the time domain analysis generally used in evaluating the response of soil deposits under vertical propagation of a horizontal shear wave (SH-wave). The finite element

*Corresponding author. *E-mail address:* hiennghiem@ssisoft.com (Hien, N. M.)

method is robust in the nonlinear analysis of a dynamic problem in the time domain. In the 1D finite element analysis, a soil column is discretized into a series of the spring elements approximated by Kelvin-Voight solid, whereby represented by modulus and viscous damping. The nonlinear seismic site response analysis required a cyclic nonlinear constitutive soil model described the relationship between stress and strain in the soil deposit. Several cyclic nonlinear models have been developed, and all are characterized by 1) a backbone curve; 2) unloading-reloading behavior, stiffness degradation and other effects; and 3) generation of the excess pore water pressure during cyclic excitation [2].

A backbone curve can describe the performance of the cyclic nonlinear model. From test data, a satisfactory agreement was found that a simple hyperbolic law can adequately describe the backbone curve for small strains. The hyperbolic model proposed by Kondner [3] is probably the most frequently used model in soil static and dynamics. The analogy to the hyperbolic law for larger strains was proposed by Duncan and Chang [4] and Hardin and Drnevich [5] and the modified hyperbolic model proposed by Phillips and Hashash [2]. Cyclic behavior of soils is governed by four rules [1]: 1) for initial loading, the stress-strain curve follows the backbone curve; 2) the Masing rule is used for unloading and reloading curves with a factor of 2 is applied to the backbone curve; 3) if unloading or reloading curve crossed the backbone curve, the stress-strain curve would follow the backbone curve until the next reversal; 4) if an unloading or reloading curve passed an unloading or reloading curve from the previous cycle, it would follow that of unloading or reloading curve until the next reversal. When applying the Masing rule, hysteretic damping at large strains is overestimated [2]. To overcome this shortcoming, Darendeli [6] proposed a factor to reduce the size of hysteretic loops to match damping curves obtained from laboratory tests. Phillips and Hashash [2] formulated a reduction factor and non-Masing unloading-reloading rules for the modified Kondner-Zelasko model (MKZ) [7] in the 1D site response analysis. They named it as the Modulus Reduction Damping Factor (MRDF) model. Groholsky et al. [8] developed a simplified model for small-strain nonlinearity and strength, the general quadratic/hyperbolic (GQ/H) model in the 1D seismic site response analysis. In this soil model, new non-Masing unloading-reloading rules were also applied based on the MRDF approach. Because the application of MRDF behavior to other 1D backbone formulations is difficult, Numanoglu et al. [9] presented a generalized MRDF-type non-Masing hysteresis model that can apply widely to any backbone formulation for use in cyclic analysis in 1D, 2D, or 3D stress spaces.

In this study, the proposed model overcomes the following shortcomings of the current models 1) softening behavior of the backbone curve; 2) stress-dependent parameters for stress-strain relationship and damping.

2. Review of 1-D finite element analysis for site response

2.1. 1-D finite element model

A multi-degree-of-freedom 1D finite element model was adopted to model the geologic column, as shown in Fig. 1. The dynamic soil properties include maximum shear modulus, damping factor, and density. The 1D element, a thin Kevin-Voigt solid, is represented by a lumped mass, nonlinear spring, and dashpot for viscous damping that can be determined from the dynamic soil properties (Fig. 2). In the finite element model, a fixed base is applied if using within motion while the elastic half-space should be selected if using outcrop motion [10, 11]. The viscous damping coefficient is assumed to be proportional to the product of the mass density and shear wave velocity for the elastic half-space as in the following equation:

$$C_E = \rho_E V_{SE} \tag{1}$$

where ρ_E is the density; and V_{SE} is the shear wave velocity of the elastic half-space.

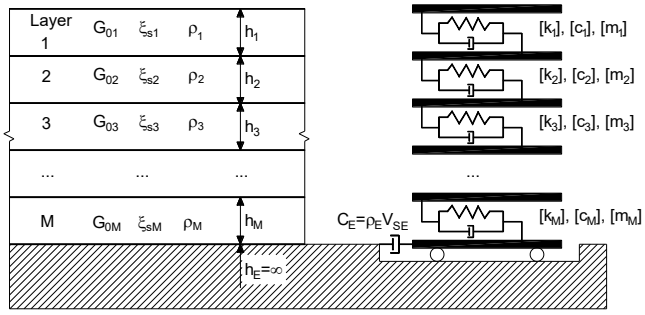

Figure 1. The 1D model for site response analysis

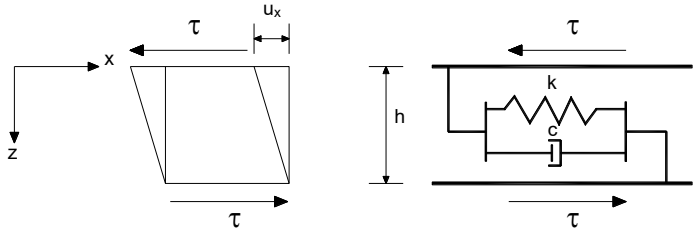

Figure 2. A thin element of Kevin-Voigt solid [1]

2.2. *Stress-strain relationship and hysteretic damping*

Eqs. (2) and (3) define the initial loading and unloading-reloading, respectively in the nonlinear stress-strain relationship of soil as follows [2]:

$$\tau = \frac{G_0 \gamma}{1 + \beta(\gamma/\gamma_r)^r} \tag{2}$$

$$\tau = \tau_{rev} + \frac{2G_0\left[(\gamma - \gamma_{rev})/2\right]}{1 + \beta\left[(\gamma - \gamma_{rev})/2\gamma_r\right]^r} \tag{3}$$

where γ and τ are given shear strain and shear stress, respectively; r is dimensionless exponent; γ_r is shear strain parameter; G_0 is maximum shear modulus; β is a dimensionless factor; and γ_{rev} and τ_{rev} are reversal shear strain and shear stress, respectively.

The hysteretic damping is related to the energy lost and the peak energy stored in a cycle of vibration for an equivalent linear material (Fig. 3):

$$\xi_h = \frac{\Delta W}{4\pi W} \tag{4}$$

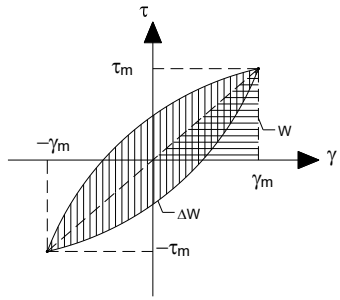

Figure 3. Relationship between hysteresis loop and damping ratio [1]

where W is peak energy and ΔW is dissipated energy in one cycle.

Currently, most of the available stress-strain relationships are using the Masing rule for unloading-reloading curves. The hysteretic damping using the Masing rule applied to the stress-strain relationship for unloading-reloading from medium to large strains is higher than that obtained in a dynamic test [2, 6]. This difference leads to an underestimation of shear strain because of higher energy dissipation in the analysis model. The parameters of the soil model need to be calibrated using both shear modulus reduction and damping curves to overcome this mismatch. Darendeli [6] proposed a reduction factor that effectively alters the Masing rules to provide a better match for both shear modulus reduction and damping curves simultaneously. The following hysteretic damping using a reduction factor was proposed [6]:

$$\xi_{nm} = DF\left(\gamma_m\right)\xi_m \tag{5}$$

where ξ_m is hysteretic damping calculated from a looping curve using the Masing rule based on the modulus reduction curve; $DF\left(\gamma_m\right)$ is Darendeli' reduction factor dependent on stress level as follows:

$$DF\left(\gamma_m\right) = b_1\left(\frac{\sigma'}{\sigma'_{ref}}\right)^{c_1} \tag{6}$$

where σ' is effective stress; σ'_{ref} is reference effective stress; b_1 is variable which depends on the soil and input motion properties and $c_1 = 0.1$.

Phillips and Hashash [2] also developed a new expression for a damping reduction factor which modified the Masing rule and provided a better match with the damping curves for larger strains. A trial and error procedure obtained this proposed function. Eq. (7) presents the unloading and reloading stress-strain relationship when applying the damping reduction factor:

$$\tau = F\left(\gamma_m\right)\left\{2\frac{G_0\left[\left(\gamma-\gamma_{rev}\right)/2\right]}{1+\beta\left[\left(\gamma-\gamma_{rev}\right)/2\gamma_r\right]^r} - \frac{G_0\left(\gamma-\gamma_{rev}\right)}{1+\beta\left(\gamma_m/\gamma_r\right)^r}\right\} + \frac{G_0\left(\gamma-\gamma_{rev}\right)}{1+\beta\left(\gamma_m/\gamma_r\right)^r} + \tau_{rev} \tag{7}$$

where γ_m is maximum shear strain; $F\left(\gamma_m\right)$ is Phillips and Hashash' damping reduction factor determined as follows:

$$F\left(\gamma_m\right) = p_1 - p_2\left(1 - \frac{G_{\gamma_m}}{G_0}\right)^{p_3} \tag{8}$$

where p_1, p_2, and p_3 are non-dimension parameters selected to obtain the best fit with a damping curve; G_{γ_m} is secant shear modulus at the maximum shear strain, γ_m. Other equations for the unloading and reloading stress-strain relationship with the damping reduction factor can be found in Groholski et al. [8] and Hashash et al. [12].

3. The proposed independent-stress parameters

3.1. Stress-strain relationship

a. Backbone curve

A new hyperbolic equation for the backbone curve is developed based on the hyperbolic model proposed by Kondner and Zelasko [7]. A parameter r, added to adjust the shape of the backbone curve, produces an equation similar to the model developed by Matasovic [13] given in the following form:

$$\tau = \frac{G_0\gamma}{1+\left(\gamma/\tilde{\gamma}_r\right)^r} \tag{9}$$

where $\tilde{\gamma}_r$ is shear strain parameter. Eq. (9) can be rearranged as:

$$\log\left(\frac{G_0}{G_s}-1\right)=r\log\left(\gamma\right)-r\log\left(\tilde{\gamma}_r\right) \tag{10}$$

Eq. (10) presents a straight line based on the dynamic soil data of G_s/G_0 versus shear strain. The value of r is the slope of the best fit straight line, and the value $-r\log\left(\tilde{\gamma}_r\right)$ can be determined from the intercept between the best fit straight line and the vertical axis. The ordinary least-squares method can in finding the best fit straight line.

Rearranging Eq. (9) in the following form:

$$\tau=\frac{\gamma}{\frac{1}{G_0}+\gamma^r\Big/G_0\Big(\tilde{\gamma}_r\Big/\beta^{\frac{1}{r}}\Big)^r} \tag{11}$$

The term $\tilde{\gamma}_r/\beta^{\frac{1}{r}}$ is constant so that it can be assigned as $\gamma_r=\tilde{\gamma}_r/\beta^{1/r}$.

The backbone curve in Eq. (11) can be written in a new form as follows:

$$\tau=\frac{\gamma}{\dfrac{1}{G_0}+\dfrac{\gamma^t}{\tau_u}} \tag{12a}$$

where t is a dimensionless exponent; τ_u is ultimate shear stress, $\tau_u=\bar{\gamma}_r G_0$.

If $r\leq 1$ then

$$t=r \text{ and } \bar{\gamma}_r=\gamma_r^r \tag{12b}$$

If $r>1$ then

$$t=1 \text{ and } \bar{\gamma}_r=\gamma_r(r-1)^{1-\frac{1}{r}} \tag{12c}$$

Eq. (12c) is developed to avoid softening behavior beyond the peak shear stress when, $r>1$ as shown in Fig. 4.

b. Unloading-Reloading Formulation

The general equation for unloading-reloading is given as follows:

$$\tau=\tau_{rev}+f_{\gamma_m}\frac{\gamma-\gamma_{rev}}{\dfrac{1}{G_0}+\dfrac{\left(|\gamma-\gamma_{rev}|\right)^t}{2^t\tau_u}}+\left(1-f_{\gamma_m}\right)\left(\gamma-\gamma_{rev}\right)G_s \tag{13}$$

where f_{γ_m} is damping reduction factor, and the reloading and unloading equations are similar to the backbone curve if the turning point $(\tau_{rev},\gamma_{rev})$ is considered as their original coordinates.

c. Stress-independent parameters for backbone curves

The maximum shear modulus is dependent on confining stress, as shown in the following equation:

$$G_0=G_{0,ref}\left(\frac{\sigma_c'+\sigma_{c,0}'}{\sigma_{c,ref}'}\right)^{\eta_g} \tag{14}$$

where $\sigma_{c,ref}'$ is reference effective confining stress, usually taken as atmospheric pressure; $G_{0,ref}$ is maximum shear modulus at the reference confining stress; σ_c' is effective confining stress; η_g is modulus exponent; and $\sigma_{c,0}'$ is reference effective confining stress at $z=0$, which is added to the original equation to avoid zero value of G_0 at $z=0$.

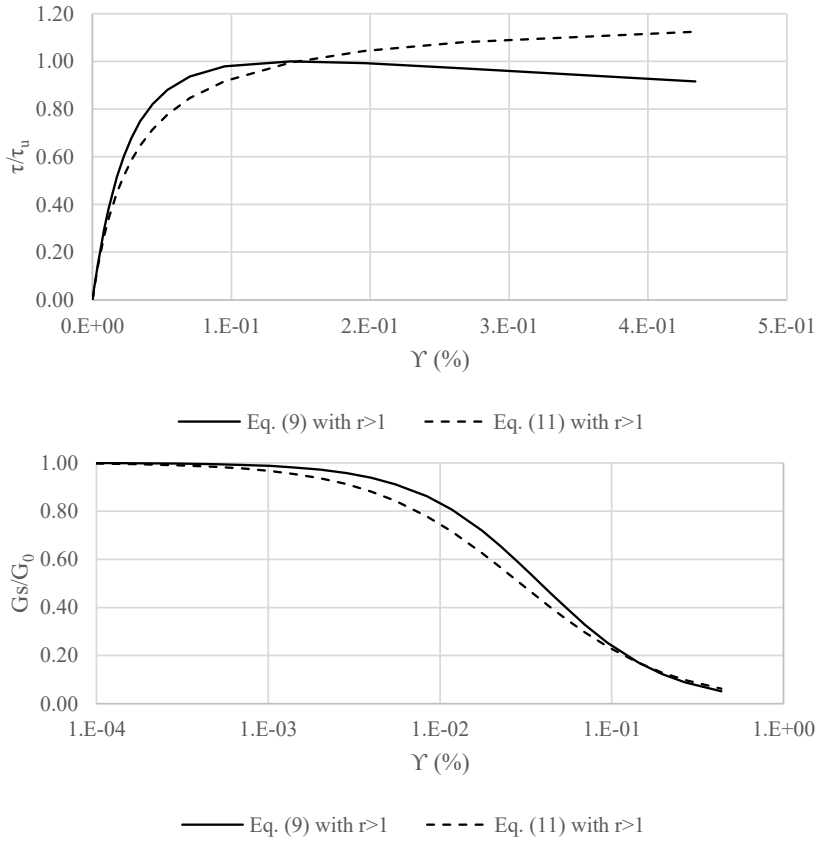

Figure 4. Effect of r value on the backbone curve shape

The following expression is adopted to represent the dependence of the reference shear strain on the confining stress:

$$\gamma_r = \gamma_{ref}\left(\frac{\sigma'_c + \sigma'_{c,0}}{\sigma'_{c,ref}}\right)^{\eta_\gamma} \tag{15}$$

where γ_{ref} is reference shear strain at the reference confining stress; and η_γ is reference shear strain exponent.

3.2. Hysteretic damping

In this study, a new equation for the reduction factor for the unloading-reloading rule is proposed. The hysteretic damping of a cyclic loop is expressed as:

$$\xi_h = \frac{\Delta W}{W} \tag{16}$$

where ΔW is the dissipated energy per motion cycle and W is the strain energy.

Consider a loop shown in Fig. 3, based on the backbone curve, the shear stress at the first reversal point is given by:

$$\tau_m^{(+)} = \frac{G_0\gamma_m^{(+)}}{1 + \left(\gamma_m^{(+)}/\gamma_r\right)^t} \tag{17}$$

where γ_m is a maximum reversal shear strain corresponding to the hysteretic damping, ξ_h.

The ratio of the secant and maximum shear moduli can be obtained from Eq. (21) as:

$$\frac{G_s}{G_0} = \frac{1}{1 + \left(\gamma_m^{(+)} / \gamma_r\right)^t} \tag{18}$$

where G_s is secant shear modulus.

With $\gamma_{rev} = \gamma_m^{(+)}$ and $\tau_{rev} = \tau_m^{(+)}$, Eq. (13) becomes:

$$\tau = \tau_m^{(+)} - f_{\gamma_m} \frac{\gamma_m^{(+)} - \gamma}{\frac{1}{G_0} + \frac{\left|\gamma_m^{(+)} - \gamma\right|^t}{2^t \tau_u}} - \left(1 - f_{\gamma_m}\right)\left(\gamma_m^{(+)} - \gamma\right) G_s \tag{19}$$

The dissipated energy per motion cycle and the strain energy are computed by:

$$\Delta W = 2 \int_{\gamma_m^{(-)}}^{\gamma_m^{(+)}} \left[\tau_m^{(+)} - \tau - G_s\left(\gamma_m^{(+)} - \gamma\right)\right] d\gamma \tag{20}$$

$$W = \frac{\bar{\gamma}_m^2 G_s}{2} \tag{21}$$

where $\bar{\gamma}_m = \dfrac{\gamma_m^{(+)} - \gamma_m^{(-)}}{2}$.

Substituting Eqs. (20) and (21) into Eq. (16) leads to:

$$\xi_h = \frac{\Delta W}{4\pi W} = 2^t \bar{\gamma} \frac{G_0}{G_s} \frac{f_{\gamma_m}}{\pi \bar{\gamma}_m^2} \int_{\gamma_m^{(-)}}^{\gamma_m^{(+)}} \frac{\gamma_m^{(+)} - \gamma}{2^t \bar{\gamma} + \left|\gamma_m^{(+)} - \gamma\right|^t} d\gamma - f_{\gamma_m} \frac{2}{\pi} \tag{22}$$

The following equation can approximate a small strain damping from a damping curve:

$$\xi_s = \xi_{\gamma_{\min}} - \xi_{h,\gamma_{\min}} \tag{23}$$

where $\xi_{\gamma_{\min}}$ is hysteretic damping from a damping curve at $\gamma_{\min}$ (minimum shear strain in a damping curve); $\xi_{h,\gamma_{\min}}$ is hysteretic damping at $\gamma_{\min}$.

The damping reduction factor f_{γ_m} is applied to obtain the best fit between the modified hysteretic damping and the damping curve as follows:

$$\xi_{mh} = 2^t \bar{\gamma} \frac{G_0}{G_s} \frac{f_{\gamma_m}}{\pi \bar{\gamma}_m^2} \int_{\gamma_m^{(-)}}^{\gamma_m^{(+)}} \frac{\gamma_m^{(+)} - \gamma}{2^t \bar{\gamma} + \left|\gamma_m^{(+)} - \gamma\right|^t} d\gamma - f_{\gamma_m} \frac{2}{\pi} \tag{24}$$

The relationship between the modified hysteretic damping, small strain damping, and hysteretic damping from damping curve is given by:

$$\xi_{mh} = \xi_c - \xi_s \tag{25}$$

where ξ_c is the hysteretic damping determined from a damping curve.

By rearranging Eq. (24), the damping reduction factor is obtained as:

$$f_{\gamma_m} = \frac{\xi_c - \xi_s}{2^t\bar{\gamma}\dfrac{G_0}{G_s}\dfrac{f_{\gamma_m}}{\pi\bar{\gamma}_m^2}\displaystyle\int_{\gamma_m^{(-)}}^{\gamma_m^{(+)}}\frac{\gamma_m^{(+)}-\gamma}{2^t\bar{\gamma}+\left|\gamma_m^{(+)}-\gamma\right|^t}d\gamma - \frac{2}{\pi}} \tag{26}$$

a. Stress-independent parameters

The soil model parameters for hysteretic damping are also stress-independent and determined from the damping curves. The stress-independent parameters are denoted by subscription "ref" determined at the reference confining stress , which is usually taken as 101.3 kPa.

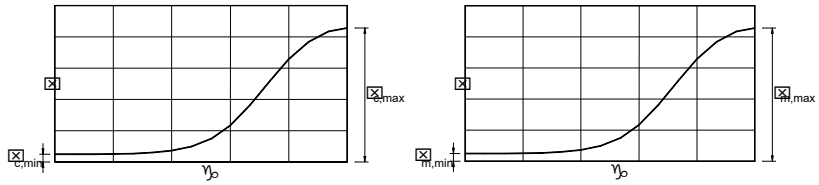

Figure 5. Typical hysteretic damping curves

The damping curve, small strain damping, and the Masing hysteretic damping are stress-dependent parameters that can be written in terms of reference parameters. For example, the following equation presents an approximation of the damping curve (Fig. 5):

$$\xi_c = \xi_{c,ref}\left(\frac{\sigma'_c + \sigma'_{c,0}}{\sigma'_{c,ref}}\right)^{\eta_{\xi_c}}\left(1 - \frac{1}{1+\lambda_{ref}\left(\dfrac{\sigma'_c+\sigma'_{c,0}}{\sigma'_{c,ref}}\right)^{\eta_\lambda}(\gamma/\gamma_r)^u}\right) + \xi_s \tag{27}$$

where u, η_{ξ_c}, and η_λ are best-fitting parameters; λ_{ref} is a reference best-fitting parameter; and $\xi_{c,ref}$ is a reference hysteretic damping from the damping curve calculated as:

$$\xi_{c,ref} = \xi_{c,\max,ref} - \xi_{c,\min,ref} \tag{28}$$

where $\xi_{c,\max,ref}$ and $\xi_{c,\min,ref}$ maximum and minimum hysteretic damping values determined from the damping curve.

The small strain damping is also dependent on the confining stress as the following expression:

$$\xi_s = \xi_{s,ref}\left(\frac{\sigma'_c + \sigma'_{c,0}}{\sigma'_{c,ref}}\right)^{\eta_{\xi_s}} \tag{29}$$

where $\xi_{s,ref}$ is a reference small strain damping; η_{ξ_s} is a best-fitting exponent. The Masing hysteretic damping formulation is given in the same form as the hysteretic damping from the damping curve (Fig. 5):

$$\xi_m = \xi_{m,ref}\left(\frac{\sigma'_c + \sigma'_{c,0}}{\sigma'_{c,ref}}\right)^{\eta_{\xi_m}}\left(1 - \frac{1}{1+\alpha_{ref}\left(\dfrac{\sigma'_c+\sigma'_{c0}}{\sigma'_{c,ref}}\right)^{\eta_\alpha}(\gamma/\gamma_r)^s}\right) \tag{30}$$

where η_{ξ_m}, $s$and η_α are best-fitting parameters; $\xi_{m,ref}$ is reference Masing hysteretic damping; and α_{ref} is a reference best-fitting parameter.

Based on the variation of the damping reduction factor with the maximum reversal shear strain, γ_m in Eq. (26), the damping reduction factor can be approximated as follows:

$$f_{\gamma_m} = \frac{\xi_c - \xi_s}{\xi_m} = \frac{\bar{\xi}_{c,ref}}{\bar{\xi}_{m,ref}} \frac{\lambda}{\alpha} \frac{1 + \alpha(\gamma/\gamma_r)^s}{1 + \lambda(\gamma/\gamma_r)^u} (\gamma/\gamma_r)^{u-s} \tag{31}$$

4. Implementation of new equations

The proposed equations of stress-independent parameters are implemented in the computer program SRAP (Soil Response Analysis Program). The soil parameters can be determined automatically from the shear modulus reduction and damping curves. The procedure used to determine the model parameters consists of the following steps: 1) Determine the pressure-dependent parameters to fit the shear modulus reduction curves; 2) determine the small strain damping parameters; 3) calculate damping factors using backbone parameters and the unloading-reloading rules; 4) predict the damping reduction factor based on damping curves and damping factors calculated in step 3; 5) estimate the stress-dependent parameters of the reduction factor in Eq. (31).

The viscous damping in the finite element analysis is frequency-independent viscous damping developed by Nghiem and Chang [14], which can be determined from the small strain damping ratios of the soils.

5. Model verification

5.1. Shear modulus reduction and damping curves

Table 1 presents the model parameters determined by using the above procedure for selected shear modulus reduction and damping curves studied by Vucetic and Dobry [15] and Darendeli [6]. A curve set from Vucetic and Dobry [15] is stress-independent then all scalar parameters are zero. Darendeli [6] a set of 20 curves for soils with different plastic indexes and confining stresses. Dependences of

Table 1. Soil parameters

Parameters	Vucetic and Dobry [15]						Darendeli [6]				
	PI = 0	PI = 15	PI = 30	PI = 50	PI = 100	PI = 200	PI = 0	PI = 15	PI = 30	PI = 50	PI = 100
$\gamma_{r,ref}$ (%)	0.030	0.078	0.150	0.262	0.572	0.862	0.033	0.046	0.062	0.081	0.129
η_γ	0.000	0.000	0.000	0.000	0.000	0.000	0.377	0.290	0.383	0.379	0.388
r	1.064	0.903	0.916	0.917	1.098	1.060	0.908	0.915	0.910	0.912	0.909
$\xi_{s,ref}$ (%)	1.081	1.049	1.005	0.949	0.892	0.828	0.834	1.041	1.247	1.521	2.204
η_{ξ_s}	0.000	0.000	0.000	0.000	0.000	0.000	−0.312	−0.312	−0.312	−0.312	−0.312
η_{ξ_c}	0.000	0.000	0.000	0.000	0.000	0.000	−0.028	−0.042	−0.053	−0.066	−0.093
$\xi_{c,ref}$ (%)	26.659	24.611	23.245	20.401	15.968	14.292	19.815	19.375	18.909	18.302	16.937
λ_{ref}	0.420	0.608	0.701	0.777	1.060	1.060	0.759	0.741	0.775	0.802	0.869
u	0.793	0.764	0.747	0.717	0.715	0.679	0.982	0.975	0.977	0.978	0.983
η_λ	0.000	0.000	0.000	0.000	0.000	0.000	0.013	−0.049	0.058	0.068	0.129
η_{ξ_m}	0.000	0.000	0.000	0.000	0.000	0.000	−0.059	−0.047	−0.097	−0.102	−0.138
$\xi_{m,ref}$ (%)	61.769	48.949	48.301	45.943	50.265	46.064	43.355	41.747	39.670	37.433	33.258
α_{ref}	0.331	0.382	0.408	0.452	0.545	0.595	0.488	0.523	0.566	0.614	0.720
s	0.944	0.896	0.918	0.929	1.011	1.019	0.928	0.937	0.937	0.942	0.943
η_α	0.000	0.000	0.000	0.000	0.000	0.000	0.095	0.075	0.130	0.134	0.167

the reference shear strain, small strain damping, and damping reduction factor on the confining stress represented by non-zero scalar parameters.

Fig. 6 shows comparisons of modulus reduction and damping curves between the proposed model and Darendeli [6]. Only the curves of sandy soil with plastic index PI = 0 are plotted. It can be seen that the agreement is excellent for all curves.

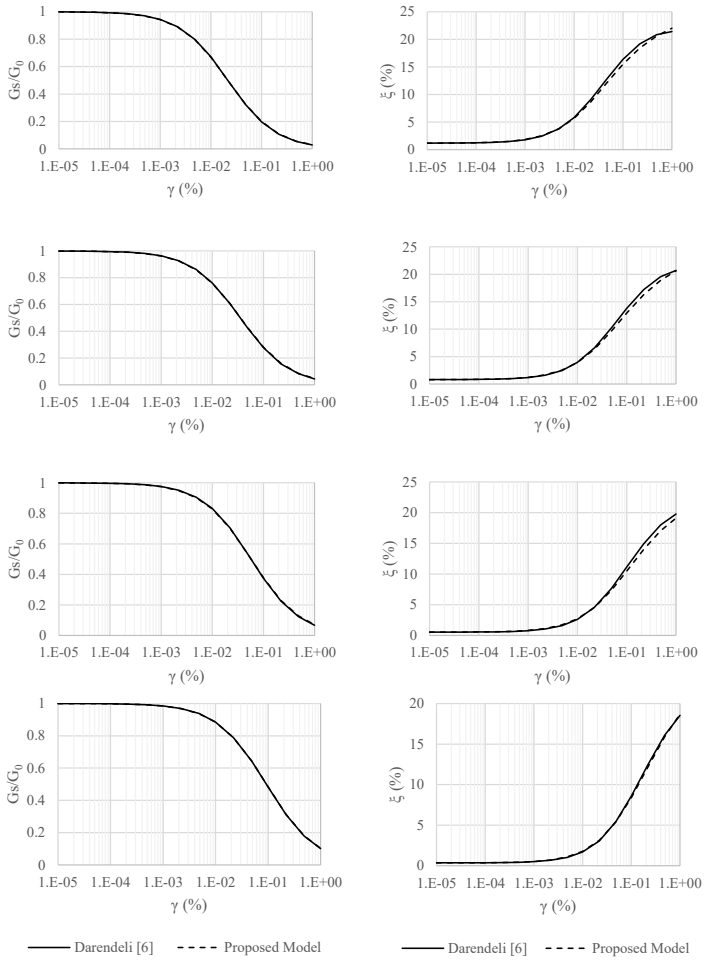

Figure 6. Comparison of shear modulus reduction and damping curves

5.2. 1D site response analysis using stress-independent parameters

1D site response analysis using stress-independent parameters is performed for comparisons with centrifuge experiments conducted at the University of Colorado, Boulder centrifuge facility [16]. The soil used in the test was Nevada Sand (No. 120) with a unit weight of 15.4 kN/m^3 and a friction angle of 330. The shear wave velocity profile predicted as the average of the empirical procedures [16] was presented in Fig. 7 with the corresponding maximum shear modulus profile. The shear modulus reduction and damping curve was obtained from Darendeli's curves for $PI = 0$ and reconstructed at different confining pressures corresponding to 0 m, 6.5 m, 13.5 m, 18 m, and 25 m [16]. In the analysis model, only one set of stress-independent parameters obtained from the above curves describes the

dynamic properties of the soil, as presented in Table 2. The values of the small strain damping vary from 1.76% to 0.54% that close to the values used by Hashash et al. [16] (Fig. 8). The shear modulus reduction and damping curves at different depths matched very well to those used in Deepsoil analyses [16] (Fig. 9). The stress-independent parameters provide implied friction angles at large strain (10%) in good agreement with the target friction angle [16] at 0 m, 6.5 m, 13.5 m, and 19 m. However, the discrepancy between the implied friction angle and the target friction angle is about 16% at 25 m, as shown in Fig. 10.

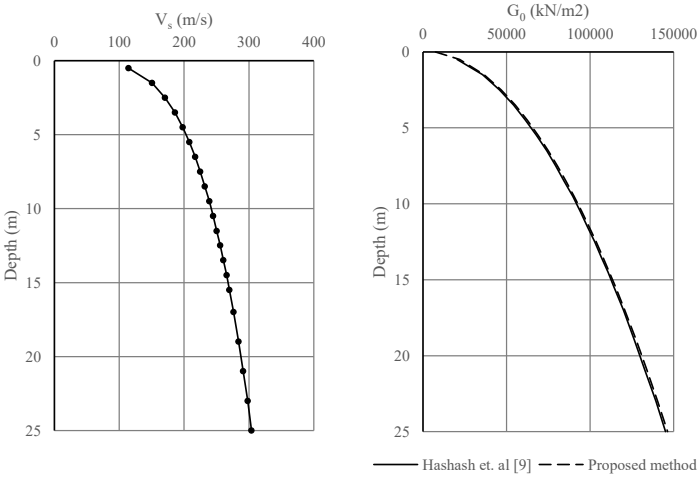

Figure 7. Shear wave velocity (V_s) and shear modulus (G_0) profiles

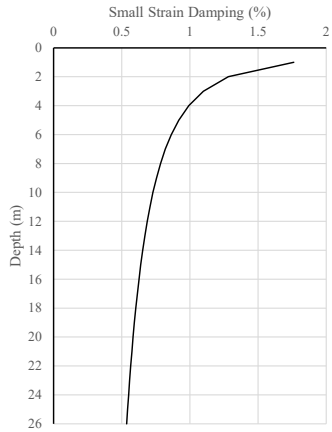

Figure 8. Small strain damping profile

Table 2. Soil parameters used in the site response analyses

Parameters	Values	Parameters	Values	Parameters	Values
$G_{0,ref}$ (kPa)	75000	η_{ξ_s}	−3.119E−1	η_{ξ_m}	−2.656E−2
η_g	0.5	η_{ξ_c}	8.036E−3	$\xi_{m,ref}$ (%)	37.511
$\gamma_{r,ref}$ (%)	3.340E−2	$\xi_{c,ref}$ (%)	20.416	α_{ref}	0.565
η_γ	3.996E−1	λ_{ref}	0.893	s	0.872
r	0.818	u	0.896	η_α	−2.810E−3
$\xi_{s,ref}$ (%)	0.820	η_λ	0.054		

Two representative ground motions were selected in the analyses because of their lowest and highest peak ground acceleration (PGA) [16]. The selected ground motions named LomaSCZ with PGA of 0.33 g and KobeTAK with PGA of 0.76 g are shown in Fig. 11. In the 1D finite element model, the soil column is discrete into 26 elements with a uniform element size of 1 m. The results of the site response analyses using Srap program include the maximum displacement, PGA, maximum shear strain profiles, and 5%-damped surface acceleration response spectra. The comparisons of the results between Srap, Deepsoil nonlinear analyses [16], and the centrifuge measurements [16] were shown Figs. 12 and 13.

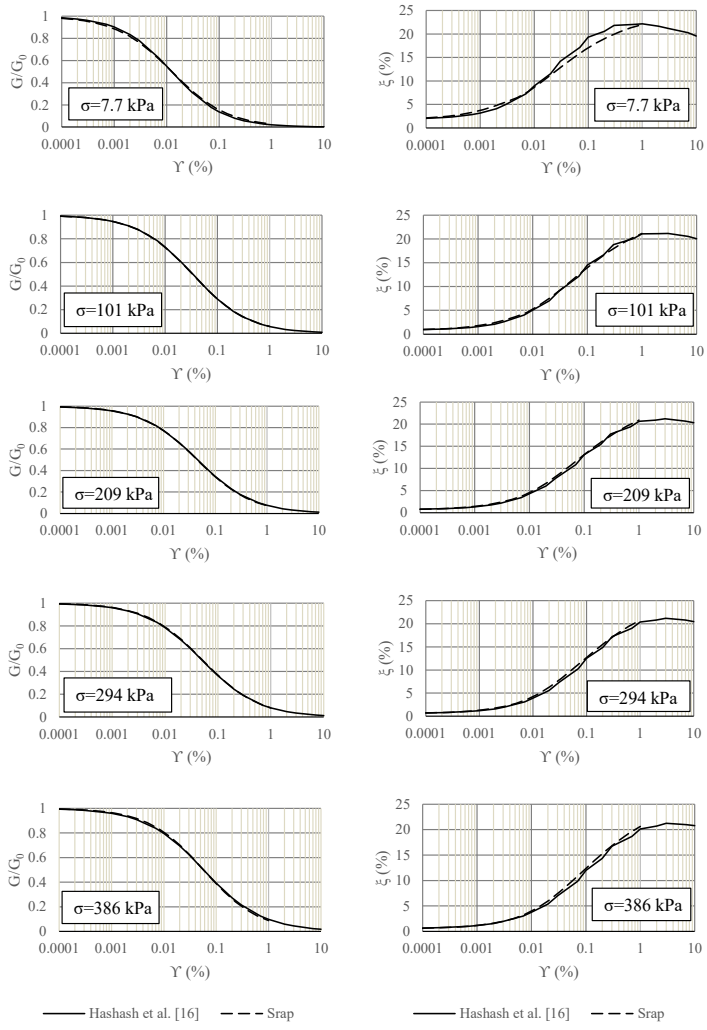

Figure 9. Comparison of shear modulus reduction and damping curves

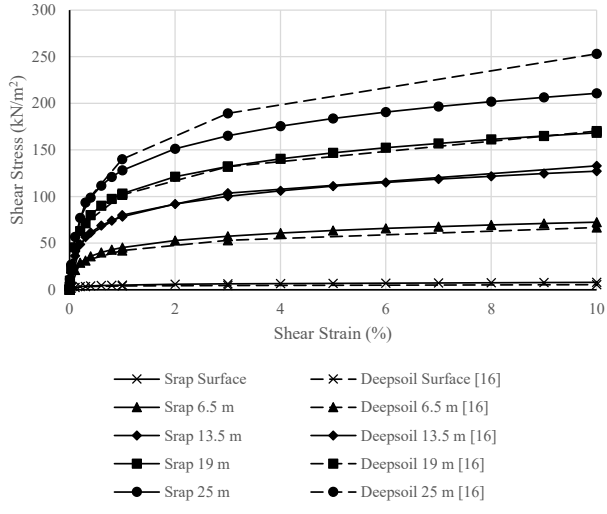

Figure 10. Stress-strain curves used in the analyses

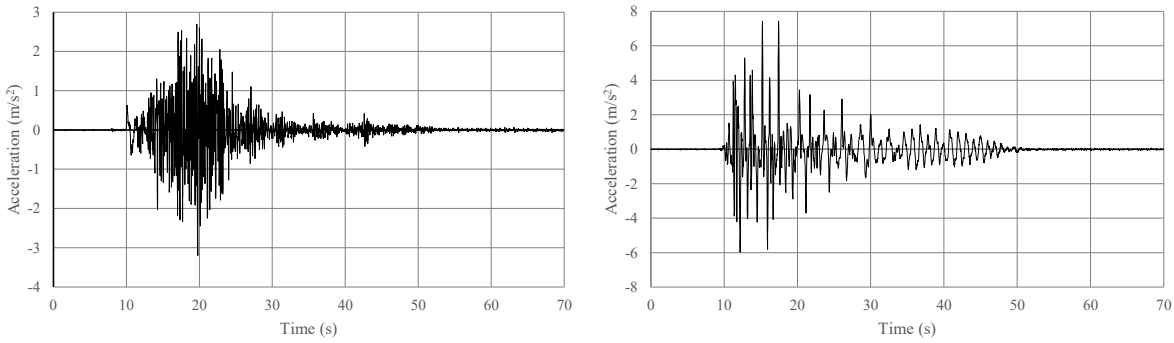

(a) LomaSCZ motion (b) KobeTAK motion

Figure 11. Base motions [16]

Fig. 12 shows the comparisons of the site response between centrifuge experiment, Deepsoil [16], and Srap during the LomaSCZ motion. The calculated maximum displacement profiles from both Deepsoil and Srap agreed very well with those from the centrifuge measurements. Deepsoil and Srap

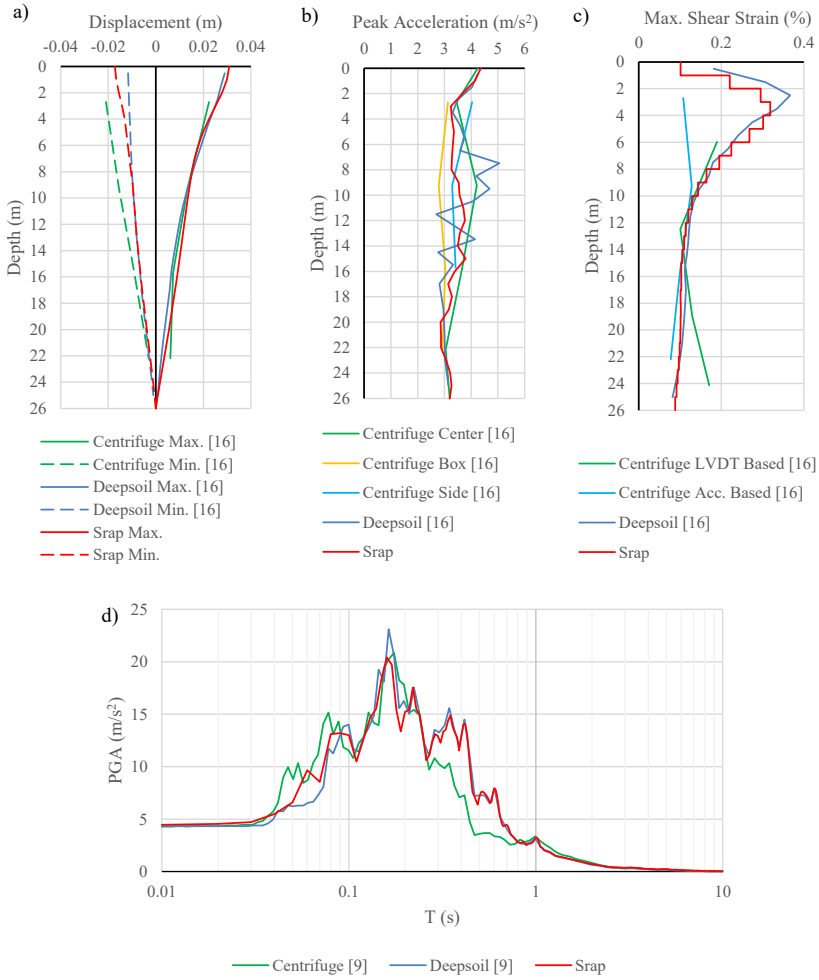

Figure 12. Comparison between predictions and centrifuge measurements during the LomaSCZ motion

also produced a good match with each other for the minimum displacement profiles below the depth of 4 m, but those values are much smaller than the centrifuge measurements (Fig. 12(a)). The predicted PGA values from Srap fell in between the measurements from the central and box accelerometer arrays (Fig. 12(b)). However, above 3 m and below 22 m, perfect matches were obtained for all prediction results in comparison to the measurements from the central accelerometer array. For the maximum shear strain comparison, the best predictions were observed at a depth below 6 m for both Deepsoil and Srap results. Above that depth, the predictions were overestimated (Fig. 12(c)). The surface acceleration response spectra created from Deepsoil and Srap compared well with that measured in the centrifuge experiment except that they produced underestimated predictions in period ranged from 0.03 s to 0.1 s and overestimated predictions in period ranged from 0.3 s to 0.8 s.

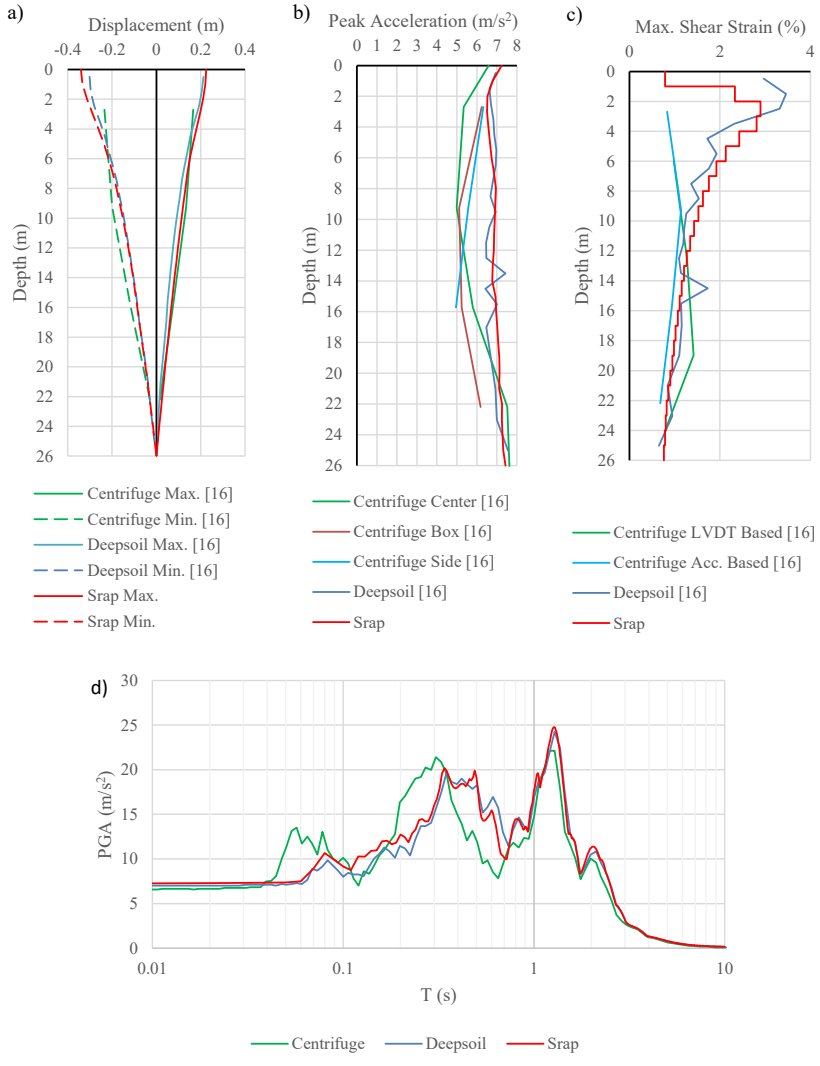

Figure 13. Comparison between predictions and centrifuge measurements during the KobeTAK motion

During the KobeTAK motion, both maximum and minimum displacement profiles predicted by Deepsoil and Srap agreed well with the centrifuge measurements (Fig. 13(a)). In terms of PGA comparison, although the predictions were very close to each other, they overestimated the centrifuge

measurements. The best matches were only observed near the surface and below 22 m (Fig. 13(b)). The maximum shear strain profiles were compared in Fig. 13(c) with a fair agreement for all results below 10 m. Both predictions provided the same shape of the maximum shear strain distribution above 10 m, but they were overestimation in comparison to the measurements. The predictions of the surface acceleration response spectra agreed quite well to each other for all ranges of periods, as shown in Fig. 12(d). A good agreement between predictions and measurements found beyond a period of 0.7 s. Below that period, the predictions were underestimated.

6. Conclusions

New formulations for stress-strain relationship and hysteretic damping were developed to model the nonlinear behavior of 1D seismic site response analysis. The proposed backbone and unloading-reloading equations can simultaneously be matched shear modulus reduction and damping curves proposed by Vucetic and Dobry [15] and Darendeli [6]. In the proposed soil model, the backbone curve was represented by the modified hyperbolic model, and a damping reduction factor was introduced to adjust the unloading-reloading curve such that hysteretic damping matched more closely to the measured damping.

The proposed formulations for stress-strain relationship and hysteretic damping are implemented in the finite element code SRAP. The formulations were validated through numerical site response analyses with reference to the measurements of the free field seismic response at the ground surface and different depths of the centrifuge experiments. The results of the numerical analysis were compared with another computer program, and the measurements in terms of maximum and minimum displacement, peak acceleration, maximum shear strain profiles, and response spectra. The conclusion can be made that using the proposed model for 1D finite element analysis in the time domain using proposed stress-independent parameters can produce reliable results in comparison to the model tests.

References

[1] Kramer, S. L. (1996). *Geotechnical earthquake engineering*, volume xviii. Upper Saddle River, NJ: Prentice Hall.

[2] Phillips, C., Hashash, Y. M. A. (2009). Damping formulation for nonlinear 1D site response analyses. *Soil Dynamics and Earthquake Engineering*, 29(7):1143–1158.

[3] Kondner, R. L. (1963). Hyperbolic stress-strain response: cohesive soils. *Journal of the Soil Mechanics and Foundations Division*, 89(1):115–143.

[4] Duncan, J. M., Chang, C.-Y. (1970). Nonlinear analysis of stress and strain in soils. *Journal of Soil Mechanics & Foundations Div*, 96:1629–1653.

[5] Hardin, B. O., Drnevich, V. P. (1972). Shear modulus and damping in soils: measurement and parameter effects. *Journal of Soil Mechanics & Foundations Div*, 98:667–692.

[6] Darendeli, M. B. (2001). *Development of a new family of normalized modulus reduction and material damping curves*. Ph. D., Civil Engineering, University of Texas at Austin.

[7] Kondner, R. L. (1963). A hyperbolic stress-strain formulation for sands. In *Proceedings of the 2nd Pan American Conference on Soil Mechanics and Foundation Engineering, Brazil*, volume 1, 289–324.

[8] Groholski, D. R., Hashash, Y. M. A., Kim, B., Musgrove, M., Harmon, J., Stewart, J. P. (2016). Simplified model for small-strain nonlinearity and strength in 1D seismic site response analysis. *Journal of Geotechnical and Geoenvironmental Engineering*, 142(9):04016042.

[9] Numanoglu, O. A., Hashash, Y. M. A., Cerna-Diaz, A., Olson, S. M., Bhaumik, L., Rutherford, C. J., Weaver, T. (2017). Nonlinear 3-D modeling of dense sand and the simulation of a soil-structure system under multi-directional loading. In *Geotechnical Frontiers*, 379–388.

[10] Hashash, Y. M. A., Park, D. (2001). Non-linear one-dimensional seismic ground motion propagation in the Mississippi embayment. *Engineering Geology*, 62(1-3):185–206.

[11] Hashash, Y. M. A., Park, D. (2002). Viscous damping formulation and high frequency motion propagation in non-linear site response analysis. *Soil Dynamics and Earthquake Engineering*, 22(7):611–624.

[12] Hashash, Y. M. A., Musgrove, M. I., Harmon, J. A., Okan, I., Groholski, D. R., Phillips, C. A., Park, D. (2017). *DEEPSOIL 7.0*. User Manual.

[13] Matasovic, N. (1994). Seismic response of composite horizontally-layered soil deposits. PhD thesis, University of California, Los Angeles.

[14] Nghiem, H. M., Chang, N.-Y. (2019). A new viscous damping formulation for 1D linear site response analysis. *Soil Dynamics and Earthquake Engineering*, 127:105860.

[15] Vucetic, M., Dobry, R. (1991). Effect of soil plasticity on cyclic response. *Journal of Geotechnical Engineering*, 117(1):89–107.

[16] Hashash, Y. M. A., Dashti, S., Romero, M. I., Ghayoomi, M., Musgrove, M. (2015). Evaluation of 1-D seismic site response modeling of sand using centrifuge experiments. *Soil Dynamics and Earthquake Engineering*, 78:19–31.